Title	Abnormal variation of band gap in Zn doped Bi0.9La0.1FeO3 nanoparticles: Role of Fe-O-Fe bond angle and Fe-O bond anisotropy
Author(s)	Xu, XL; Liu, WF; Wu, P; Zhang, H; Guo, MC; Han, YL; Zhang, C; Gao, J; Rao, GH; Wang, S
Citation	Applied Physics Letters, 2015, v. 107 n. 4, article no. 042905
Issued Date	2015
URL	http://hdl.handle.net/10722/218810
Rights	Creative Commons: Attribution 3.0 Hong Kong License

Abnormal variation of band gap in Zn doped $Bi_{0.9}La_{0.1}FeO_3$ nanoparticles: Role of Fe-O-Fe bond angle and Fe-O bond anisotropy

Xunling Xu,[1] Weifang Liu,[1,a)] Ping Wu,[1] Hong Zhang,[1] Minchen Guo,[1] Yuling Han,[1] Chuang Zhang,[2] Ju Gao,[3] Guanghui Rao,[4] and Shouyu Wang[2,3,a)]
[1]*Tianjin Key Laboratory of Low Dimensional Materials Physics and Preparing Technology, School of Science, Tianjin University, Tianjin 300072, China*
[2]*College of Physics and Materials Science, Tianjin Normal University, Tianjin 300074, China*
[3]*Department of Physics, The University of Hong Kong, Pokfulam Road, Hong Kong*
[4]*Department of Information Materials Science and Engineering, Guilin University of Electronic Technology, Guilin 541004, Guangxi, China*

(Received 29 May 2015; accepted 19 July 2015; published online 28 July 2015)

$Bi_{0.9}La_{0.1}FeO_3$ (BLFO) and $Bi_{0.9}La_{0.1}Fe_{0.99}Zn_{0.01}O_3$ (BLFZO) nanoparticles were prepared via a sol-gel method. The oxygen vacancies and holes increase with Zn doping analyzed through X-ray photoelectron spectroscopy, which could contribute to the increase of leakage current density. However, with the increase of the defects (oxygen vacancies and holes), the band gap of BLFZO also is increased. To explain the abnormal phenomenon, the bandwidth of occupied and unoccupied bands was analyzed based on the structural symmetry driven by the Fe-O-Fe bond angle and Fe-O bond anisotropy. © *2015 AIP Publishing LLC*. [http://dx.doi.org/10.1063/1.4927644]

In recent years, significant attention has been paid to magnetoelectric (ME) multiferroics which display the potential applications in advanced spintronic and ME devices.[1–4] The multiferroic materials possess both ferroelectric and ferromagnetic (or antiferromagnetic) ordering within a single phase. Among all the multiferroic materials studied so far, $BiFeO_3$ (BFO) exhibits high ferroelectric Curie temperature ($T_C \sim 1103$ K) and high G-type antiferromagnetic Néel temperature ($T_N \sim 643$ K),[5] which make it one of the prime candidates for room-temperature ME applications.

In addition to the above-mentioned applications, BFO is also considered as a kind of visible-light-responsive photocatalyst due to its suitable band gap (2.1–3.0 eV) and excellent chemical stability. For example, Gao *et al.*[6] reported that BFO nanoparticles could be used as an efficient photocatalyst for the degradation of methyl orange. Hengky *et al.*[7] demonstrated the active visible-light photochemical behavior of BFO nanoparticles in combination with rapid decolourisation of Rhodamine B. Furthermore, being a semiconductor with suitable band gap, BFO will have other prospective applications such as solar cells and optoelectronic devices. In 2010, Yang *et al.*[8] investigated the solar cells which take advantage of the narrow band gap of BFO thin films. In a report by Ji *et al.*,[9] the bulk photovoltaic effect in the visible wavelength with BFO thin films was further studied. For the applications mentioned here, the band gap is of particular importance, as it determines the optical and electrical properties. It is noteworthy that the band gap of BFO can be influenced by the crystalline size. For instance, Wang *et al.*[10] reported the increase in band gap of BFO nanoparticles with decreasing crystalline size (within the range of 80–500 nm), and they have thought that the variation may be due to the quantum-size effect. However, Mocherla *et al.*[11] demonstrated that the band gap of BFO nanoparticles decreased with decreasing particle size (from 85 nm to 5 nm), which was attributed to the increasing microstrain with decreasing size. Additionally, the common defects such as oxygen vacancies and holes also are important factors that control the band gap of BFO, because the defects as impurity-induced energy levels usually can lead to the decrease of band gap.[11] Therefore, by controlling the densities of defects, a significant tuning of the band gap can be realized in BFO.

Cation substitutions for both A and B sites in BFO have been shown to modulate the density of defects,[12–14] where the effects of doping on the optical and electrical properties can be utilized. Nonmagnetic ion Zn^{2+} has a stable ionic charge. The effects of Zn dopant on structural, electrical, and magnetic properties for BFO thin films have been reported.[15–17] The reports demonstrated that the introduction of Zn is an effective way to enhance the ferroelectric behavior of BFO films. However, the effects of Zn doping on the optical properties for BFO nanoparticles have seldom been reported. In this study, we have studied the electrical and optical properties of $Bi_{0.9}La_{0.1}FeO_3$ (BLFO) and $Bi_{0.9}La_{0.1}Fe_{0.99}Zn_{0.01}O_3$ (BLFZO) nanoparticles, where the 10% La was added to stabilize the single phase. Due to charge neutrality, the substitution of divalent Zn^{2+} at trivalent Fe-site can easily increase the number of oxygen vacancies and holes, which results in the high leakage current of BLFZO. The defects also can play an important role in the optical properties, because they produce the impurity band between the valence band and conduction band, which can narrow the band gap. While interestingly, with Zn substitution, the band gap of BLFZO is increased although the oxygen vacancy and hole are increased. To explain this, we consider the effects of structural symmetry on the band gap based on the Fe-O-Fe bond angle and Fe-O bond anisotropy.

BLFO and BLFZO nanoparticles were synthesized by sol-gel method. Appropriate amounts of $Bi(NO_3)_3{\cdot}5H_2O$, $Fe(NO_3)_3{\cdot}9H_2O$, $La(NO_3)_3{\cdot}6H_2O$, and $Zn(NO_3)_2{\cdot}6H_2O$ were

a)Authors to whom corresponding should be addressed. Electronic addresses: wfliu@tju.edu.cn and shouyu.wang@yahoo.com.

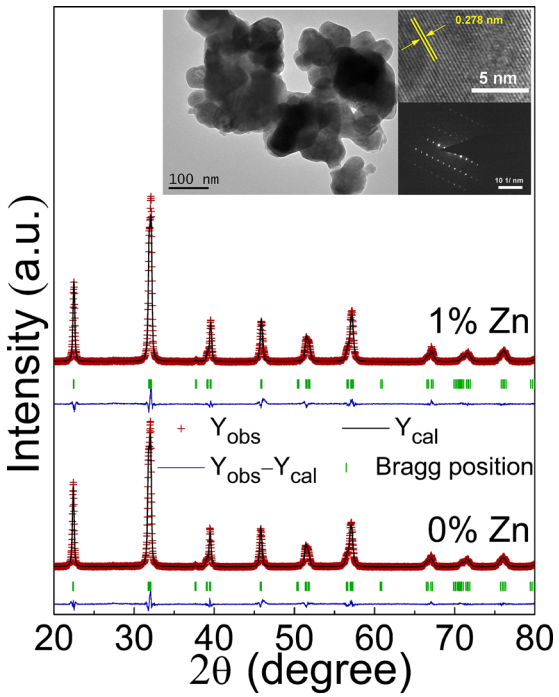

FIG. 1. Rietveld refined XRD pattern of BLFO and BLFZO nanoparticles. The inset shows TEM images of BLFZO sample.

dissolved in ethylene glycol. Tartaric acid in 1:1 molar ratio with respect to metal cation was added to the solution, and the mixture was stirred at 70 °C for 3 h. The obtained solution was dried at 90 °C for 3 h until it was turned to yellowish-brown gel. The gel was further dried at 140 °C for 3 h, then annealed at 400 °C for 1.5 h, and finally ground into powders. Subsequently, the powders were calcined for 2 h at 550 °C to obtain samples. The as-prepared samples have no retained carbon introduced by ethylene glycol and tartaric acid, which can be confirmed from the thermogravimetry analysis (TGA) data (supplementary material (Fig. S1)[18]).

The crystalline structure analysis of samples was carried out by X-ray diffraction (XRD) (Rigaku D/MAX-2500 diffractometer with Cu Kα radiation). The microstructural properties were investigated by transmission electron microscopy (TEM), high resolution TEM (HRTEM), and the corresponding selected area electron diffraction (SAED) pattern using JEM-2100F instrument. To analyze the chemical states of Fe ions, X-ray photoelectron spectroscopy (XPS) was recorded with PHI1600. UV-vis absorption spectrum of the samples was performed by Shimadzu UV-3600 UV-VIS-NIR spectrophotometer. To study the electrical properties, the samples were pressed into pellets, and the pellets were sintered for half an hour at 500 °C. The dielectric properties were measured by a precise impendence analyzer WK 6400 with an ac signal of 1000 mV. The leakage current curve was evaluated using an Axiacct model TF 2000 ferroelectric analyser. All the measurements were carried out at room temperature.

The Rietveld refined XRD patterns of the samples are shown in Fig. 1, and the results indicate that all the main XRD peaks can be well fitted with a single-phase perovskite structure of R3c. The structural parameters obtained from the Rietveld refinement are given in Table I. It is evident from Table I that the lattice parameters of BLFZO are larger than those of BLFO, which is expected since the radius of Zn^{2+} ion (radius = 0.74 Å) is larger than that of Fe^{3+} ion (radius = 0.645 Å).[15] In addition, from the enlarged view of the diffraction peaks located at about $2\theta = 32°$ (Fig. S2 of supplementary material[18]), it can be observed that the diffraction peak has an obvious shift toward low degree with doping, which confirms that Zn is successfully doped into the BLFO matrix. The TEM image of BLFZO is shown in the inset of Fig. 1. From the TEM image, it is observed that the shape of most particles is spherical, but some of them are irregular, and some agglomerations in nature are found. The average particle size obtained from TEM image for the sample lies between 40 and 70 nm. The upper and lower insets of the TEM image show the HRTEM image and SAED pattern of an individual BLFZO nanoparticle, respectively, which indicate the single-crystalline nature of our samples with high degree of crystallinity.

Figure 2 shows the UV-vis absorption spectra of the samples. It can be observed that the samples can absorb considerable amount of visible light suggesting their potential application as visible-light photocatalyst. The band gap E_g for the samples can be calculated by using the Tauc relation: $(\alpha h\nu)^2 = A(h\nu - E_g)$,[19] where A is a constant, $h\nu$ is the photon energy, and α is absorption coefficient. The corresponding plots of $(\alpha h\nu)^2$ versus $h\nu$ for samples were prepared and the value of the band gap was estimated by the linear extrapolation approach, which are shown in the inset (a) of Fig. 2. From the inset (a), it can be seen that the band gap of BLFO nanoparticles is estimated to be 2.13(84) eV, which is close to previously reported band gap value.[7] While, with Zn substitution, the band gap is increased (2.17(26) eV for BLFZO), which indicates that Zn doping has a significant influence on the optical properties of our nanoparticles. As generally reported,[11] the existence of defect-induced energy levels between the conduction and valence bands can lead to the decrease of band gap. In BFO, the oxygen vacancy impurity band locates at the bottom of conduction band as a kind of donor level and the hole as acceptor band locates at the top of valence band. These defects can reduce the band gap since the densities of oxygen vacancy donor and hole acceptor are increased in acceptor-cation doped BFO.[14] In our case, however, the band gap is increased with the substitution of divalent Zn, which seems against the general acceptor-cation doping. Moreover, the samples' particle size observed by SEM (supplementary material (Fig. S3)[18]) has no significant difference. As a result, the effects of crystalline size and microstrain on the abnormal variation of band

TABLE I. Structure parameters obtained from Rietveld refinement of BLFO and BLFZO samples.

Modes	a (Å)	c (Å)	Unit cell volume (Å^3)	Fe-O-Fe (deg)	Fe-O1/Fe-O2 (Å)
BLFO	5.5721(5)	13.8039(1)	371.17	156.64	1.96/2.08
BLFZO	5.5736(6)	13.8058(7)	371.43	155.30	1.89/2.14

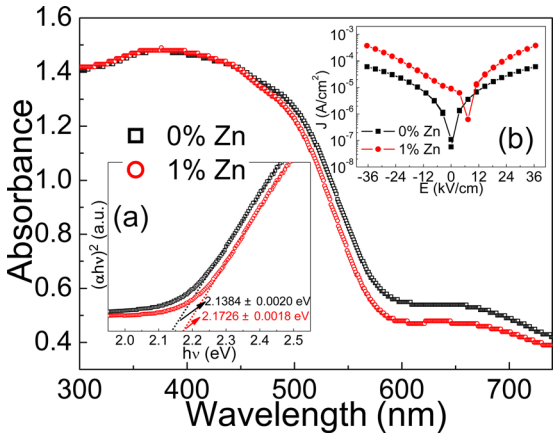

FIG. 2. UV-vis absorption spectrum of BLFO and BLFZO nanoparticles. Inset (a) $(\alpha h\nu)^2$ versus $h\nu$ plot of both samples. Inset (b) leakage current density (J) as a function of applied electric field (E) for the samples.

gap are expected to be very small. In order to systematically investigate the optical properties, the valence band spectra and core levels of elements were studied by XPS.

The XPS spectra analyses of the Bi 4f, Fe 2p, and O 1s core level regions were shown in Figs. 3(a)–3(c), respectively, where the core level binding energies were aligned with respect to C 1s peak (284 eV). As can be seen from Fig. 3(a), in both samples, Bi $4f_{7/2}$ and Bi $4f_{5/2}$ were observed at 158.49 eV and 163.81 eV, respectively. The spin-orbital splitting energy of Bi 4f is 5.32 eV, which confirms the existence of Bi^{3+}.[20] The peaks related with the Bi^{2+}, which were reported elsewhere,[21] are absent here. In Fig. 3(b), the Fe 2p core level regions were fitted and the results show that the Fe^{3+} oxidation state coexists with Fe^{2+} oxidation state. The binding energy peak position of Fe $2p_{3/2}$ located at about 709.5 eV (olive line) is attributed to the Fe^{2+}, and the position of Fe $2p_{3/2}$ located at about 710.9 eV (blue line) is ascribed to the Fe^{3+}.[22] According to the fitting, the ratio of Fe^{3+}:Fe^{2+} is calculated to be 9.6 and 7.3 for BLFO and BLFZO, respectively, indicating the increase of Fe^{2+} ions with Zn substitution. In Fig. 3(c), the XPS spectra of O 1s

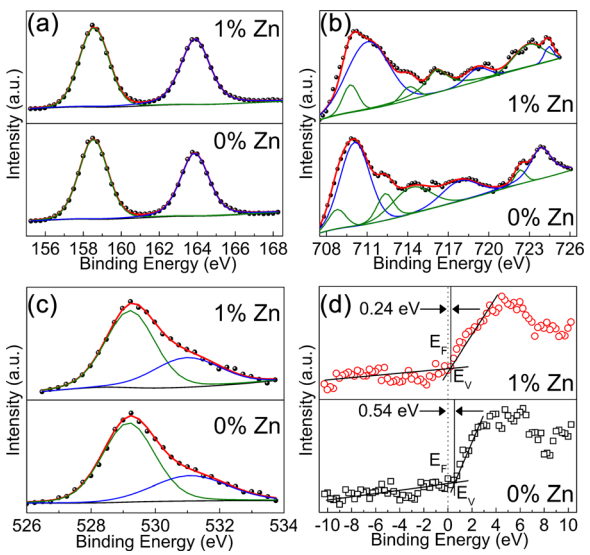

FIG. 3. The XPS spectra of (a) Bi 4f, (b) Fe 2p, and (c) O 1s for BLFO and BLFZO nanoparticles; (d) the XPS valence band spectra of BLFO and BLFZO samples.

show two peaks at about 529.2 eV and 531.1 eV, respectively. The former (olive line) is attributed to the intrinsic O^{2-} ions at the lattice sites, while the latter (blue line) is related to the oxygen deficient regions.[23] By calculating the ratio of area under the two peaks obtained from fitting the O 1s spectra, the results reveal that the oxygen vacancy concentration is effectively increased with Zn doping. The XPS valence band spectra of samples are shown in Fig. 3(d). From these data, we estimate the separation between the valence-band energy (E_V) and the Fermi energy (E_F) to be 0.54 eV and 0.24 eV for BLFO and BLFZO, respectively. It can be seen clearly that the position for the E_V is shifted to a lower binding energy region by about 0.3 eV in BLFZO sample, demonstrating a shift of E_F to valence band. Consequently, the XPS valence band spectra indicate that the Zn doping leads to the remarkable enhancement of hole concentration, which can be further confirmed by the Hall effect measurement (Table SI of supplementary material[18]). According to above comprehensive analysis, the oxygen vacancy and hole are simultaneously increased with Zn substitution, which is consistent with that observed in other Zn doped BFO crystal.[12] In fact, the substitution of divalent ion at trivalent Fe-site can easily increase the concentration of oxygen vacancy and hole. The main processes can be described as follows:

In BLFZO sample, the hole ($h^{\bullet}$) is introduced directly to compensate the charge balance upon the doping of acceptor Zn, according to

$$ZnO \rightarrow (Zn_{Fe})' + O_O^{\times} + h^{\bullet}. \quad (1)$$

The oxygen vacancy (V_O) could be easily created by loss of oxygen from the contiguous oxygen during sintering at high temperature,[24] according to

$$O_O^{\times} \rightarrow V_O + \frac{1}{2}O_2. \quad (2)$$

Therefore, Zn substitution increases the oxygen vacancy (V_O) and hole ($h^{\bullet}$). In addition, the leakage current density (J) curves of samples were also measured, as shown in the inset (b) of Fig. 2. From the J-E curves, a significant increase in leakage current of BLFZO was observed as compared to BLFO. It is well known that in the perovskite structure materials containing titanate, the ionization process of the oxygen vacancy (V_O) will create the conducting electrons,[24] and the process are described by

$$V_O \rightarrow V_O^{\bullet} + e', \quad (3)$$

$$V_O^{\bullet} \rightarrow V_O^{\bullet\bullet} + e'. \quad (4)$$

Thus, the Zn substitution increases the ionized oxygen vacancy ($V_O^{\bullet}$ or $V_O^{\bullet\bullet}$), the conducting electron (e'), and the hole ($h^{\bullet}$) eventually, which is responsible for the high leakage current of BLFZO. So far, comparing the wide band gap to the increased defects and subsequent higher leakage current, we conclude that the increase of the band gap of BLFZO requires a further analysis.

To better understand the increase of band gap and meanwhile the increase of defects with Zn substitution, the structural symmetry associated with the Fe-O-Fe bond angle and

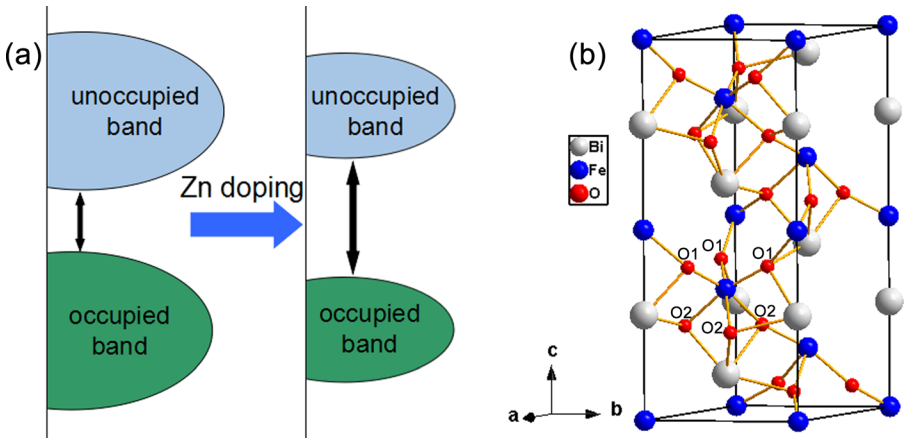

FIG. 4. (a) The schematic diagram of the change in bandwidth of occupied and unoccupied bands. (b) A schematic drawing of the refined hexagonal unit-cell structure of BFO containing six BFO formula cells (i.e., 30 atoms), showing six FeO_6-octahedron units per hexagonal unit cell. Two distinct kinds of Fe-O bonds (Fe-O1 and Fe-O2) in the FeO_6-octahedron cage are shown in the refined structure, whereby three oxygen ions located at the upper half region (along the c axis) of the FeO_6 cage belong to "O1," and the three remaining oxygen ions at the lower half region of the FeO_6 cage belong to "O2."

Fe-O bond anisotropy is discussed. As reported, BFO is a charge transfer-type material in which the conduction band is mainly composed of Fe 3d orbitals and the valence band is made of O 2p orbitals.[13] So, the Fe-O-Fe bond is important because it can control the orbital overlap between Fe and O,[4] and as such it may influence the band gap of BFO. In 2010, Borisevich *et al.*[25] demonstrated that the band gap of BFO with tilt-free cubic symmetry is decreased significantly by conducting both local spin-density approximation (LSDA) and LSDA + U calculations of the band structure, and they have further correlated the decrease of band gap with the increase of Fe-O-Fe bond angle (towards 180°) and subsequent higher symmetry. The increase of Fe-O-Fe bond angle can suppress the tilt of FeO_6-octahedron, which could increase interatomic hopping and therefore the bandwidth of occupied and unoccupied bands, and hence leads to the decrease of the band gap. In BLFZO nanoparticles, however, Zn doping induces the decrease of Fe-O-Fe bond angle (as shown in Table I), which in turn permits a high degree of FeO_6-octahedron tilt and, therefore, weakens the structural symmetry. The forced lower symmetry is expected to reduce the bandwidth of occupied and unoccupied bands, enhancing the band gap in the BLFZO, as shown in Fig. 4(a). In addition, the Fe-O bond anisotropy in the FeO_6-octahedron cage can also influence the structural symmetry. Fig. 4(b) presents a schematic drawing of the refined crystal structure of hexagonal unit cell for BFO, in which two distinct kinds of Fe-O bonds (Fe-O1 and Fe-O2) are shown. It can be seen from Table I, the Fe-O bond anisotropy (i.e., the difference in bond distance between Fe-O1 and Fe-O2) is increased significantly upon the Zn substitution. The observed variation in the Fe-O bond anisotropy of BLFZO predicts an increase in the local structural distortion, which indicates the decrease in structural symmetry of BLFZO. Thus, the band gap of BLFZO is increased due to the lower structural symmetry caused by the decreased Fe-O-Fe bond angle and increased Fe-O bond anisotropy.

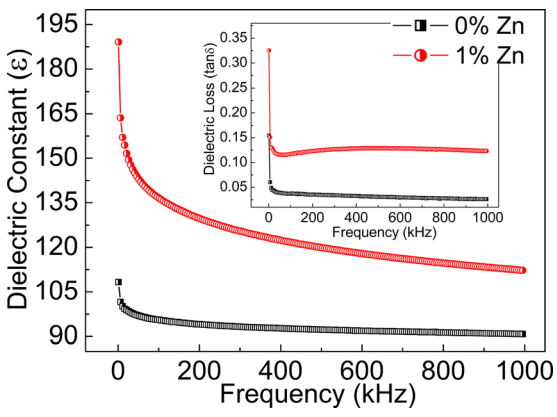

FIG. 5. The dielectric constant of BLFO and BLFZO samples at room temperature. The inset shows the dielectric loss of samples.

The room-temperature dielectric properties of samples were also investigated. As shown in Fig. 5, the dielectric constants of both samples are decreased drastically with the increase of frequency in low-frequency region (f-sensitive region) and then tend to be constant when the frequency reaches a certain value (f-stable region). This phenomenon can be well described by the Maxwell-Wagner model, which is related to the space charge relaxation.[26] The space charges (e.g., oxygen vacancies) are able to follow the frequency of the applied field at low frequencies, whereas the space charges do not find time to undergo relaxation at high frequency region.[27] Thus, the dielectric constant is observed to decrease with the increase of frequency. The higher dielectric loss is for the BLFZO sample, as observed in the inset of Fig. 5, and this may be due to the existence of many charged defects, which is in accordance with the above observations.

In summary, BLFO and BLFZO nanoparticles have been synthesized by sol-gel method. With Zn substitution, the leakage current density is enhanced due to the increase of oxygen vacancies and holes, whereas the band gap also is increased from 2.13(84) eV to 2.17(26) eV. To explain this, the structural symmetry associated with FeO_6-octahedron cage was discussed based on the Fe-O-Fe bond angle and Fe-O bond anisotropy. The increase of the band gap of BLFZO can be explained by the forced lower symmetry induced by the decreased Fe-O-Fe bond angle and increased Fe-O bond anisotropy.

This work was funded by the National Natural Science Foundation of China (Project Nos. 11004148 and 11104202), the Research Grant Council of Hong Kong (Project Nos. HKU 702112P and RGC 701813), and the Guangxi Natural Science Foundation (Grant No. 2012GXNSFGA060002).

[1]M. Bibes and A. Barthelemy, Nat. Mater. **7**, 425 (2008).
[2]Y. H. Chu, L. W. Martin, M. B. Holcomb, M. Gajek, S. J. Han, Q. He, N. Balke, C.-H. Yang, D. Lee, W. Hu, Q. Zhan, P. L. Yang, A. F. Rodriguez, A. Scholl, S. X. Wang, and R. Ramech, Nat. Mater. **7**, 478 (2008).
[3]A. Singh, V. Pandey, R. K. Kotnala, and D. Pandey, Phys. Rev. Lett. **101**, 247602 (2008).
[4]G. Catalan and J. F. Scott, Adv. Mater. **21**, 2463 (2009).
[5]J. Wang, J. B. Neaton, H. Zheng, V. Nagarajan, S. B. Ogale, B. Liu, D. Viehland, V. Vaithyanathan, D. G. Schlom, U. V. Waghmare, N. A. Spaldin, K. M. Rabe, M. Wuttig, and R. Ramesh, Science **299**, 1719 (2003).
[6]F. Gao, X. Y. Chen, K. B. Yin, S. Dong, Z. F. Ren, F. Yuan, T. Yu, Z. Zou, and J. M. Liu, Adv. Mater. **19**, 2889 (2007).
[7]C. Hengky, X. Moya, N. D. Mathur, and S. Dunn, RSC Adv. **2**, 11843 (2012).
[8]S. Y. Yang, J. Seidel, S. J. Byrnes, P. Shafer, C.-H. Yang, M. D. Rossell, P. Yu, Y.-H. Chu, J. F. Scott, J. W. Ager III, L. W. Martin, and R. Ramesh, Nat. Nanotechnol. **5**, 143 (2010).
[9]W. Ji, K. Yao, and Y. C. Liang, Adv. Mater. **22**, 1763 (2010).
[10]L. Wang, J.-B. Xu, B. Gao, A.-M. Chang, J. Chen, L. Bian, and C.-Y. Song, Mater. Res. Bull. **48**, 383 (2013).
[11]P. S. V. Mocherla, C. Karthik, R. Ubic, M. S. Ramachandra Rao, and C. Sudakar, Appl. Phys. Lett. **103**, 022910 (2013).
[12]Y. Yoneda, Y. Kitanaka, Y. Noguchi, and M. Miyayama, Phys. Rev. B **86**, 184112 (2012).
[13]K. K. Bharathi, W.-M. Lee, J. H. Sung, J. S. Lim, S. J. Kim, K. Chu, J. W. Park, J. H. Song, M.-H. Jo, and C.-H. Yang, Appl. Phys. Lett. **102**, 012908 (2013).
[14]H. Zhang, W. F. Liu, P. Wu, M. C. Guo, X. L. Xu, X. J. Xi, J. Gao, G. H. Rao, and S. Y. Wang, J. Mater. Chem. C **3**, 4141 (2015).
[15]G. D. Hu, S. H. Fan, C.-H. Yang, and W. B. Wu, Appl. Phys. Lett. **92**, 192905 (2008).
[16]Y. Y. Wang, J. Alloys Compd. **509**, L362 (2011).
[17]J. G. Wu, S. Qiao, J. Wang, D. Q. Xiao, and J. G. Zhu, Appl. Phys. Lett. **102**, 052904 (2013).
[18]See supplementary material at http://dx.doi.org/10.1063/1.4927644 for thermal analysis (TGA), enlarged view of XRD peaks ($2\theta = 32°$), SEM images, and Hall effect of samples.
[19]J. Tauc, *Amorphous and Liquid Semiconductors* (Plenum Press, New York, 1974), p. 171.
[20]J. F. Moulder, W. F. Stickle, P. E. Sobol, and K. D. Bomben, *Handbook of X-ray Photoelectron Spectroscopy* (Physical Electronics, Inc., Eden Prairie, Minnesota, 1992), p. 190.
[21]D. K. Mishra and X. D. Qi, J. Alloys Compd. **504**, 27 (2010).
[22]X. Wang, G. D. Hu, L. Cheng, C.-H. Yang, and W. B. Wu, Appl. Phys. Lett. **99**, 262901 (2011).
[23]J. C. C. Fan and J. B. Goodenough, J. Appl. Phys. **48**, 3524 (1977).
[24]C. Ang, Z. Yu, and L. E. Cross, Phys. Rev. B **62**, 228 (2000).
[25]A. Y. Borisevich, H. J. Chang, M. Huijben, M. P. Oxley, S. Okamoto, M. K. Nranjan, J. D. Burton, E. Y. Tsymbal, Y. H. Chu, P. Yu, R. Ramesh, S. V. Kalinin, and S. J. Pennycook, Phys. Rev. Lett. **105**, 087204 (2010).
[26]C. Elissalde and J. Ravez, J. Mater. Chem. **11**, 1957 (2001).
[27]H. O. Rodrigues, G. F. M. Pires Junior, J. S. Almeida, E. O. Sancho, A. C. Ferreira, M. A. S. Silva, and A. S. B. Sombra, J. Phys. Chem. Solids **71**, 1329 (2010).